4-11-2012

Ultra-soft 100 nm Thick Zero Poisson's Ratio Film with 60% Reversible Compressibility

Chieu Nguyen
University of Nebraska-Lincoln

Vivek Maheshwari
University of Waterloo

Ravi Saraf
University of Nebraska-Lincoln, rsaraf2@unl.edu

HHS Public Access

Author manuscript

Nano Lett. Author manuscript; available in PMC 2019 April 18.

Published in final edited form as:

Nano Lett. 2012 April 11; 12(4): 2171–2175. doi:10.1021/nl300686c.

Ultra-soft 100 nm Thick Zero Poisson's Ratio Film with 60% Reversible Compressibility

Chieu Nguyen, **Vivek Maheshwari**[†], and **Ravi F. Saraf**[‡]

[‡]Department of Chemical and Biomolecular Engineering, Nebraska Center for Materials and Nanoscience, University of Nebraska-Lincoln, Lincoln, NE 68512

[†]Present Address: University of Waterloo, Canada

Abstract

About a 100 nm thick multilayer film of nanoparticle monolayers and polymer layers is shown to behave like cellular-foam with a modulus below 100 KPa. The 1.25 cm radius film adhered to a rigid surface can be compressed reversibly to 60% strain. The more than four orders of magnitude lower modulus compared to its constituents is explained by considering local bending in the (nano)cellular structure, similar to cork and wings of beetles. As the rigidity of the polymer backbone is increased in just four monolayers the modulus of the composite increases by over 70%. Electro-optical map of the strain distribution over the area of compression and increase in modulus with thickness indicates the films have zero Poisson's ratio.

Graphical Abstract

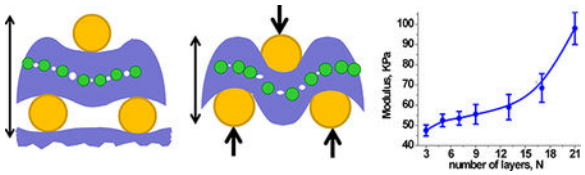

Keywords

Poisson's Ratio; Auxetic Material; Nanocomposite; Cellular Material; Sponge; Multilayer Film

Squeezing films of most solids, liquids and granular materials causes dilation in the lateral dimension which is characterized by a positive Poisson's ratio. Auxetic materials,[1] such as, special foams,[2] crumpled graphite,[3] zeolites,[4] spectrin/actin membrane,[5,6] and carbon nanotube laminates[7] shrink, i.e., their Poisson's ratio is negative. As a result of Poisson's effect, the force to squeeze an amorphous material, for example, a viscous thin film coating adhered to rigid surface increases by over million fold as the thickness decreases from 10

Contribution: CN performed the measurements and data analysis for this study, VM was involved at the early phase of the study, and RFS conceptualized the ideas, guided the study and prepared the manuscript.

Supporting Information Available:

Illustrations showing stress-strain behavior for N = 3, 7, 9, 17, and 21; and 15 nm Au particles. This material is available free of charge via the Internet at http://pubs.acs.org.

μm to 100 nm due to constrain on lateral deformations and off-plane relaxation.[8] In contrast, for zero-Poisson's ratio material, the absence of lateral deformation on bending, compressing, or extending, they can be tightly rolled or designed to make soft ultra thin film without any thickness enhancement. Due to a special cellular structure,[9] cork is a near- zero-Poisson's- ratio- material that does not dilate or contract on compression,[10] therefore it can be pressed in a wine bottle with ease to form a seal.[2] Wings of beetles also have near zero Poisson's ratio.[11] No lateral strain during flight allows the wings to morph without (energy expensive) bulging and buckling in other directions.[12] Biomimicked special cellular urethane foams are designed with zero Poisson's ratio to make morphing wings for (future) fuel efficient aircraft.[13] Gas, is an ideal zero Poisson's ratio material that, easily compresses while constrained in the lateral direction.[1] Thus, a soft, gas-like, solid thin film that can be conformally deposited on surfaces of any shape will be an effective coating for improving damping, cushioning, and traction for gripping. Especially, the soft modulus comparable to tissue (i.e., less than 100 KPa)[14] will have potential applications, for example, as coating on surgical tools to improve traction to grip delicate tissue samples with high precision for robotics and minimally invasive surgery, [15–18] as a surface coating on a complex 3D scaffold to regulate differentiation of stem cells by regulating the modulus in the 10 to 100 KPa range,[19] as a highly compressible pressure-sensitive dielectric or conductive film for tactile sensing on par with a human finger for surgical and robotic applications, [17,20–23] and as soft-cellular-structured porous coating on to 3D scaffold surface for cell proliferation[24].

We demonstrate, ultra-soft, 100 nm films of polymer/nanoparticle composite made by conventional dip coating on solid surface that can be reversibly compressed over 60% strain between rigid plates requiring (very low) stresses below 100 KPa. Using a strategy similar to cellular foams where compressive strain is distributed in the off-plane direction by local bending,[25] we demonstrate a general approach to fabricate nano-structured composite films of modulus in 30 to 100 KPa range. The modulii of individual components of the film, Au and CdS nanoparticles in a polymer matrix, are well above 1 GPa, including the polymer matrix.[26] The 10^4-fold reduction in modulus and gas-like compressibility is explained as local (reversible) bending of the polymer layer as the nanoparticles in adjacent layers interdigitate on compression.

The composite film is made by dip coating alternate layers of poly(allylamine hydrochloride) (PAH) and poly(styrene sulfonate) (PSS) followed by absorbing a monolayer of 10 nm Au or 3 nm CdS particles[27] (Fig. 1(a) and (b)). The molecular weights are 15,000 and 70,000 Daltons; and solution concentrations are 0.1% and 0.2% by weight, for PAH and PSS, respectively. The films are deposited on an Indium-Tin-Oxide (ITO) electrode on glass. The final structure is composed of three layers of Au nanoparticles and two layers of CdS nanoparticles spaced by N layers of PSS and PAH that alternate such that PAH is in contact with the nanoparticle layer or the electrode. Over 60 samples with N ranging from 3 to 21 layers are studied. The average thickness of the PSS/PAH layer, measured by ellipsometry for N = 3 to 21 layer films on Si is 1.12 nm/layer. The estimated thickness of the composite film ranges from 65 to 180 nm. The load is applied by pressing a flat Al platen onto a 12.5 mm radius optically smooth quartz disk coated with 500 nm thick Cr/Au electrode placed on the device. The Al platen is attached to a ball-and-socket joint to ensure uniform force distribution. A bias, V, is applied across the thickness of the film and the current, I, and

electroluminescence intensity, I_{el}, from CdS is recorded concomitantly as a function of applied stress, σ, to quantitatively measure the strain, ε, in the film. The "tactile image" is recorded by focusing the electroluminescent light distribution on CCD camera (instead of PMT tube) (Fig. 1(c)). The tactile image is sensitive to local modulation in electron tunneling due to local strain.[23] The uniform light in tactile image, especially closer to the edge compared to the center indicates that the stress distribution is uniform. A uniform stress distribution under no slip condition from center to the edge indicates no Poisson's effect.[8]

As the film is squeezed, the particles come closer; and both I and I_{EL} increase. The sensitivity on I-V characteristics of the device to stresses <100 KPa indicates that the modulus of the film is expected to be low (Fig. 2(a)). In contrast, the current, through a pure polymer film made of 84 layers of PSS/PAH incorporating no nanoparticles, does not exhibit any dependence on σ for the same range (Fig. 2(b)). The (expected) high toughness of pure polymer film on squeezing is typical for a solid thin film due to confinement of in-plane strain. The linear I-V behavior of the film made from just PSS and PAH is due to (ohmic) ionic current, I_N, due to the hygroscopic nature of polyelectrolytes. The ohmic current, $I_N = V/R$, where R is the (ionic) resistance. An order of magnitude higher current and nonlinear I-V behavior in the composite film, compared to pure polymer, is due to electron tunneling between the adjacent nanoparticles along the thickness direction superimposed on I_N. The nonlinear tunneling current, I_T, given by the Fowler- Nordheim equation is $I_T = P\exp(-aK/V)$, where P is proportional to the number of percolating channels, a is the tunneling distance between the particles, and K is a proportionality constant. [23,28] As a result, the total current for the composite film is given by $I = V/R + P\exp(-aK/V)$. By differentiating the I-V at fixed σ, the differential conductance, dI/dV, as a function of V is obtained (Fig. 2(c)). On extrapolating to $V \rightarrow 0$, $[dI/dV]_{V=0} = 1/R$ at various σ is estimated (Fig. 2(c) inset). As expected, R deceases monotonically as σ increases. Subsequently, by subtracting the ionic current and fitting a single exponential to V versus $I - V/R$ ($= I_t$), P and aK are determined. Interestingly, from the IT characteristics, as the film deforms, the tunneling current increases largely due to P (Fig. 2(d)) while the inter-particle distance remains nominally constant (Fig. 2(d) inset). Thus, on deformation, the rise in tunneling current occurs primarily due to a liner increase in the number of percolation channels as the particles come closer, i.e., $I_T \sim P$. Furthermore, the tunneling current is exclusively through the CdS nanoparticles; and electroluminescence only occurs due to transport through CdS, i.e., $I_{EL} \sim I_T$. Thus, a linear correspondence between $I_{EL} \sim P$ at all the σ is expected (Fig. 2(e)).

The compressive strain in the film is estimated from R. The ionic resistance is given by $R = \rho L/A$, where ρ is the resistivity, L is the film thickness, and A is the "effective" cross-sectional area for ion transport along the thickness of the film. The resistivity, $\rho \sim 1/c$, where c is a concentration of mobile ions, i.e., charge density. Assuming the number of ions does not change on compression (i.e., the lateral strain is negligible), $c \sim 1/AL$. Thus, $R \sim (1/AL)^{-1}(L/A)$, or $R \sim L^2$. Important to note is that even though A may change on deformation due to a more constricted path for ion conduction as particles come closer, the scaling $R \sim L^2$ is still valid. Considering affine deformation, the strain in the film is given by $\varepsilon_{aff} = (Ro^{0.5} - R^{0.5})/R_O^{0.5}$, where R_O is obtained by extrapolating the ionic resistance to $\sigma = 0$ (Fig. 2(c) inset). A typical stress-strain curve shows two distinct regimes: at low stress, the

deformation is linear with low modulus; and subsequently, the strain tends to flatten leading to a higher modulus similar to the densification observed in foams[25] (Fig. 3 and Fig. S1 in the Supporting Information Online (SIO)). Typical stress-strain curves for the other values of N studied among the more than 60 films tested are shown in the SIO (Fig. S1). The data at low stress-strain is difficult due to the small forces involved. Although a low friction universal joint is used to ensure flat contact, a small force is needed to "settle" the parallelism between the film and the Al platen before deformation of the film commences. Based on the data obtained for the low stress linear regime, the strains are 35% to 60% for all of the samples tested. Similar to conventional foams, at high strains, the actual strain may be smaller than ε_{aff} in the densification region.[25]

The large reversible strain with low modulus of the composite films is qualitatively explained in terms of a simple model (Fig. 4(a)). Owing to large particle density,[23] highly stratified, parallel layers of Au nanoparticles are formed (Fig. 1, SEM image). The non-conformal coating of the polymer on high density Au particle coverage leads to inter-particle voids (Fig. 4(a)). Voids in the interstitial regions have been inferred from x-reflectivity measurements on similar multilayer structure incorporating nanoparticle.[29] As the film is compressed, the larger Au nanoparticle will bend or squeeze the polymer layer containing the smaller CdS particles. The schematic, nominally to scale for N = 7 that will have a nominal thickness of ~7 nm for the PSS/PAH layers, shows ε of ~40% by local bending and squeezing of the polymer layer. As the tunneling current is exponentially sensitive to inter-particle distance, which does not change significantly (Fig. 2(d) inset), the primary mode of deformation is by bending and not squeezing. The reversibility also suggests that the film does not rupture during buckling. The deformation of the cellular structure in Fig. 4(a) is similar to cork[10] where the schematically marked nodes of the cell correspond to the location of the Au nanoparticles (Fig 4(b). Consistent with the bending, as the interposer layer gets thicker, the film becomes stiffer leading to higher modulus (Fig. 4(c), even though the amount of polymer relative to the nanoparticles increases. Conventionally, due to Poisson's effect, the lateral strain on compression is relived more effectively as thickness increases leading to lower stiffness. A reverse effect is observed in films studied: The stiffness increases monotonically with thickness in the range studied (Fig. 4(c), inset). This implies that the strain in the lateral direction is insignificant or zero, in other words, the Poisson's ratio is close to zero.

To further evaluate the validity of the bending model, the stiffness of the interposer layer is significantly reduced by eliminating CdS particles. As expected, the modulus is lowered compared to CdS-containing film (Fig. 4(d)). Furthermore, the plateau occurs at a lower stress level indicating that the pure polymer interposer layer is easier to bend at lower stress levels (Fig. 4(d) and Fig S1 in SIO). Conversely, consistent with the bending model, replacing the flexible PSS polymer with a more rigid electrolyte, heparin, the modulus is enhanced twofold. Furthermore, the modulus can be reduced by increasing the Au particle size to incorporate larger voids. For example, for N = 9, the modulus is reduced from ~55 to ~30 KPa as Au particle size increases from 10 to 15 nm (Fig. S2, SIO).

In summary, a ~100 nm thick layered film of polymer and nanoparticle monolayers is self-assembled to impart gas-like compressibility with a modulus of 50 to 100 KPa that is

comparable to tissue. The compression modulus of the film is four orders of magnitude lower than its individual constituents. The low modulus and large reversible compressibility up to 60% strain is explained by local bending of the polymer layer. The modulus of the composite film increases with film thickness. The measurements on the mechanics of the film indicate that the Poisson's ratio is zero. The films can be self-assembled by sequential dip coating process to form a soft, foam-like coating for applications, such as, improving traction to grip delicate tissues by surgical tools, sensitive tactile devices, and coatings on scaffolds for stem cell differentiation. To our knowledge, this is the first demonstration of thin films of thickness in nanometer scale that exhibit zero Poisson's ratio. The approach can be generalized to micron to centimeter scale by using larger particles and inter particle layering material.

Supplementary Material

Refer to Web version on PubMed Central for supplementary material.

Acknowledgement:

RFS thanks National Institutes of Health (R21EB008520–01) and Nebraska Research Initiative, for funding the project and supporting CN and VM.

Reference List

1. Greaves GN; Greer AL; Lakes RS; Rouxel T Poisson's ratio and modern materials. Nature Materials 2011, 10 (11), 823–837. [PubMed: 22020006]
2. Lakes R Foam Structures with A Negative Poissons Ratio. Science 1987, 235 (4792), 1038–1040. [PubMed: 17782252]
3. Wen X; Garland CW; Hwa T; Kardar M; Kokufuta E; Li Y; Orkisz M; Tanaka T Crumpled and Collapsed Conformations in Graphite Oxide Membranes. Nature 1992, 355 (6359), 426–428.
4. Grima JN; Jackson R; Alderson A; Evans KE Do zeolites have negative Poisson's ratios? Advanced Materials 2000, 12 (24), 1912–1918.
5. Schmidt CF; Svoboda K; Lei N; Petsche IB; Berman LE; Safinya CR; Grest GS Existence of A Flat Phase in Red-Cell Membrane Skeletons. Science 1993, 259 (5097), 952–954. [PubMed: 8438153]
6. Bowick M; Cacciuto A; Thorleifsson G; Travesset A Universal negative Poisson ratio of self-avoiding fixed-connectivity membranes. Physical Review Letters 2001, 87 (14).
7. Hall LJ; Coluci VR; Galvao DS; Kozlov ME; Zhang M; Dantas SO; Baughman RH Sign change of Poisson's ratio for carbon nanotube sheets. Science 2008, 320 (5875), 504–507. [PubMed: 18440923]
8. Engmann J; Servais C; Burbidge AS Squeeze flow theory and applications to rheometry: A review. Journal of Non-Newtonian Fluid Mechanics 2005, 132 (1–3), 1–27.
9. Silva SP; Sabino MA; Fernandes EM; Correlo VM; Boesel LF; Reis RL Cork: properties, capabilities and applications. International Materials Reviews 2005, 50 (6), 345–365. Also available online at www.maney.co.uk/journals/imr and www.ingentaconnect.com/content/maney/imr.
10. Grima JN; Oliveri L; Attard D; Ellul B; Gatt R; Cicala G; Recca G Hexagonal Honeycombs with Zero Poisson's Ratios and Enhanced Stiffness. Advanced Engineering Materials 2010, 12 (9), 855–862.
11. Jin T; Goo NS; Woo SC; Park HC Use of a Digital Image Correlation Technique for Measuring the Material Properties of Beetle Wing. Journal of Bionic Engineering 2009, 6 (3), 224–231.
12. Attard D; Grima JN Modelling of hexagonal honeycombs exhibiting zero Poisson's ratio. Physica Status Solidi B-Basic Solid State Physics 2011, 248 (1), 52–59.

13. Olympio KR; Gandhi F Zero Poisson's Ratio Cellular Honeycombs for Flex Skins Undergoing One-Dimensional Morphing. Journal of Intelligent Material Systems and Structures 2010, 21 (17), 1737–1753.
14. Butcher DT; Alliston T; Weaver VM A tense situation: forcing tumour progression. Nature Reviews Cancer 2009, 9 (2), 108–122. [PubMed: 19165226]
15. Dargahi J; Najarian S Human tactile perception as a standard for artificial tactile sensing - a review. International Journal of Medical Robotics and Computer Assisted Surgery 2004, 1 (1), 23–35. [PubMed: 17520594]
16. Lee MH; Nicholls HR Tactile sensing for mechatronics - a state of the art survey. Mechatronics 1999, 9 (1), 1–31.
17. Plinkert PK; Baumann I; Flemming E A tactile sensor for differentiation of tissue in minimally invasive ENT surgery. Laryngo-Rhino-Otologie 1997, 76 (9), 543–549. [PubMed: 9417183]
18. Sakai N; Tatsuta M; Yano H; Iishi H; Ishiguro S Diagnosis of the extent of gastric cancers by a new endoscopic ultrasonic tactile sensor. Gastrointestinal Endoscopy 2000, 51 (1), 69–73. [PubMed: 10625802]
19. Engler AJ; Sen S; Sweeney HL; Discher DE Matrix elasticity directs stem cell lineage specification. Cell 2006, 126 (4), 677–689. [PubMed: 16923388]
20. King CH; Culjat MO; Franco ML; Lewis CE; Dutson EP; Grundfest WS; Bisley JW Tactile Feedback Induces Reduced Grasping Force in Robot-Assisted Surgery. IEEE Transactions on Haptics 2009, 2 (2), 103–110. [PubMed: 27788101]
21. Maheshwari V; Saraf R Tactile devices to sense touch on a par with a human finger. Angewandte Chemie-International Edition 2008, 47 (41), 7808–7826. [PubMed: 18816579]
22. Crowder R Applied physics - Toward robots that can sense texture by touch. Science 2006, 312 (5779), 1478–1479. [PubMed: 16763135]
23. Maheshwari V; Saraf RF High-resolution thin-film device to sense texture by touch. Science 2006, 312 (5779), 1501–1504. [PubMed: 16763143]
24. Stevens MM; George JH Exploring and engineering the cell surface interface. Science 2005, 310 (5751), 1135–1138. [PubMed: 16293749]
25. Gibson LJ; Ashby MF Cellular Solids: Structure and Properties; Cambridge University Press, Cambridge, UK: 1997.
26. Nolte AJ; Rubner MF; Cohen RE Determining the young's modulus of polyelectrolyte multilayer films via stress-induced mechanical buckling instabilities. Macromolecules 2005, 38 (13), 5367–5370.
27. Decher G Fuzzy nanoassemblies: Toward layered polymeric multicomposites. Science 1997, 277 (5330), 1232–1237.
28. Fowler RH; Nordheim L Electon Emission in Intense Electric Fields. Proceedings of the Royal Society of London Series A. 1928, 119 (781), 173–181.
29. Cho J; Char K; Hong J-D; Lee K-B; Fabrication of Highly Ordered Multilayer Films Using a Spin Self-Assembly Method. Advance Materials. 2001, 13(14), 1076–1078.

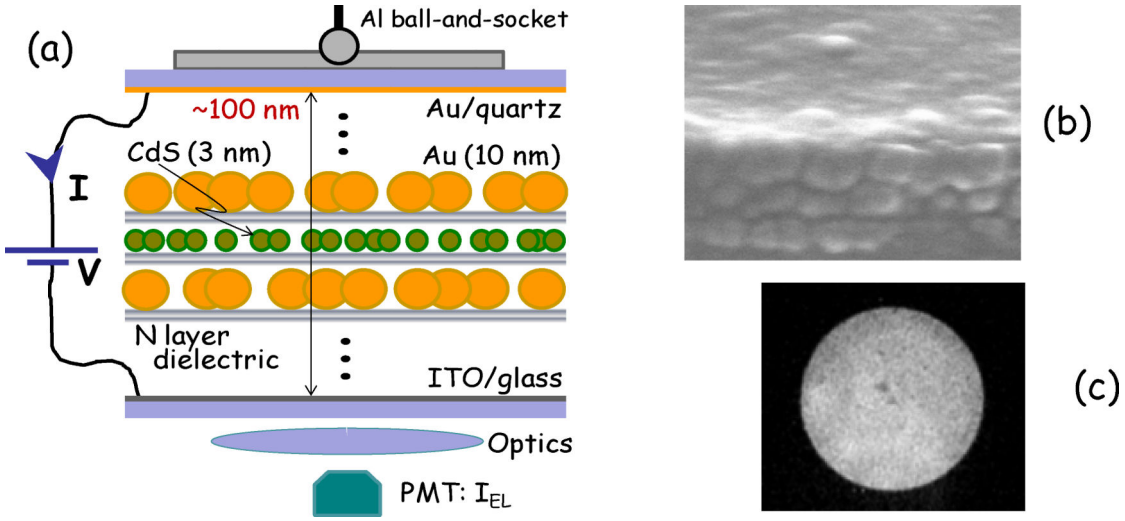

Figure 1:

(a) Schematic of electrical characterization of the device showing the load application and optical signal collection on a photomultiplier tube (PMT). Films are made with three and two monolayer of Au and CdS particles, respectively. (b) The 140 nm wide scanning electron microscope (SEM) image (with no metal deposition) shows the three 10 nm Au particle layers. The CdS particles are too small to visualize. (c) The tactile image of the quartz disk formed on the CCD camera at 40 KPa. Reproduced with permission from Reference 21. Copyright 2008 WILEY-VCH.

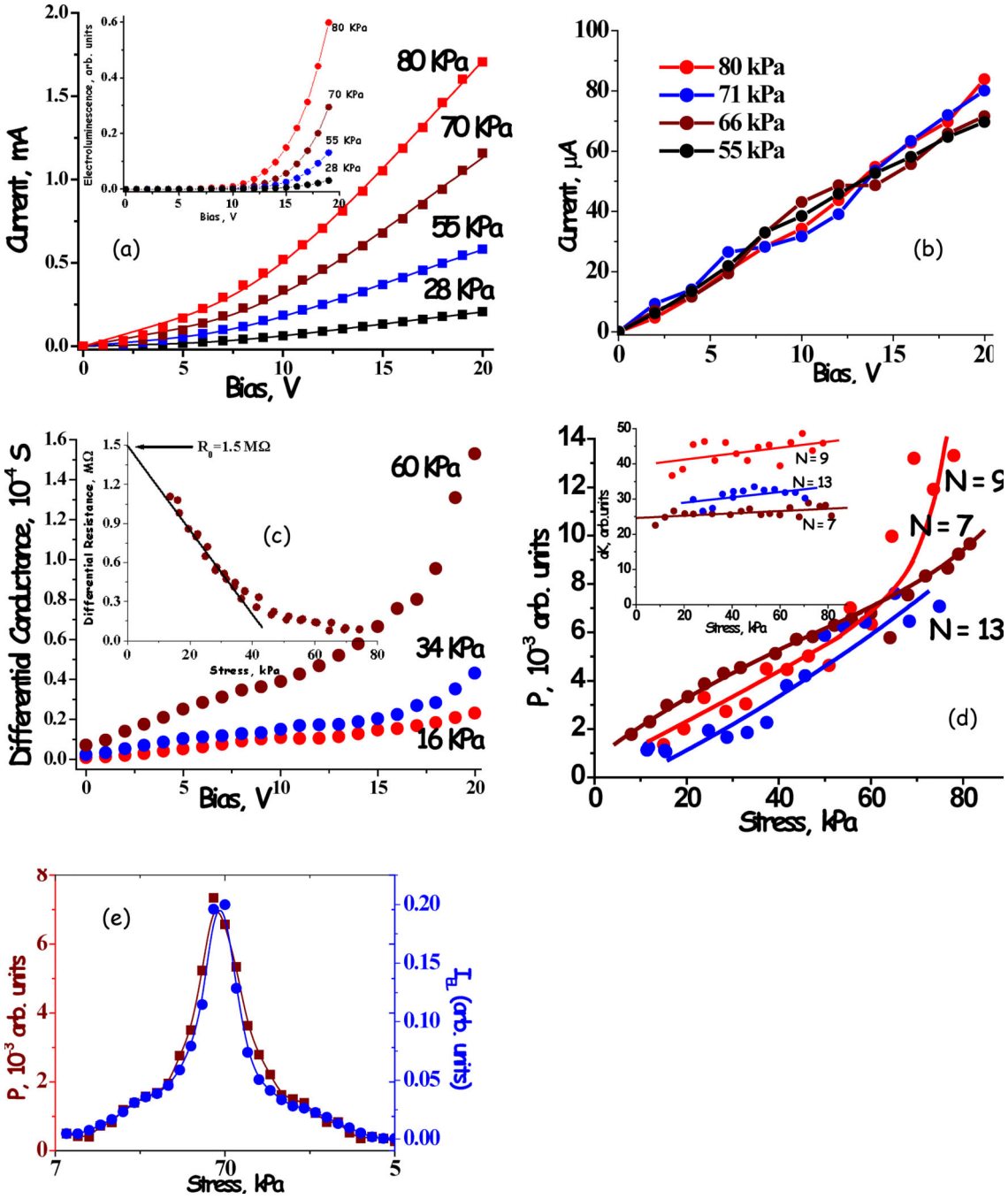

Figure 2:

Electrical response of the film on uniaxial compression. (a) A typical change in I-V response at different applied stress (N = 13). The line is a fit to the tunneling and ionic current model. Inset: Corresponding I_{EL} measured concomitantly with the I-V characterization. (b) The I-V curve does not change for PSS/PAH film (N =84 with no nanoparticles). (c) Typical effect of stress on dI/dV versus V behavior (N =5). (d) Typical behavior of tunneling parameters, P and aK, as a function of stress for three films. Each data point is based on an I-V curve at fixed. σ. (e) Typical correspondence between P and I_{EL} (N = 5).

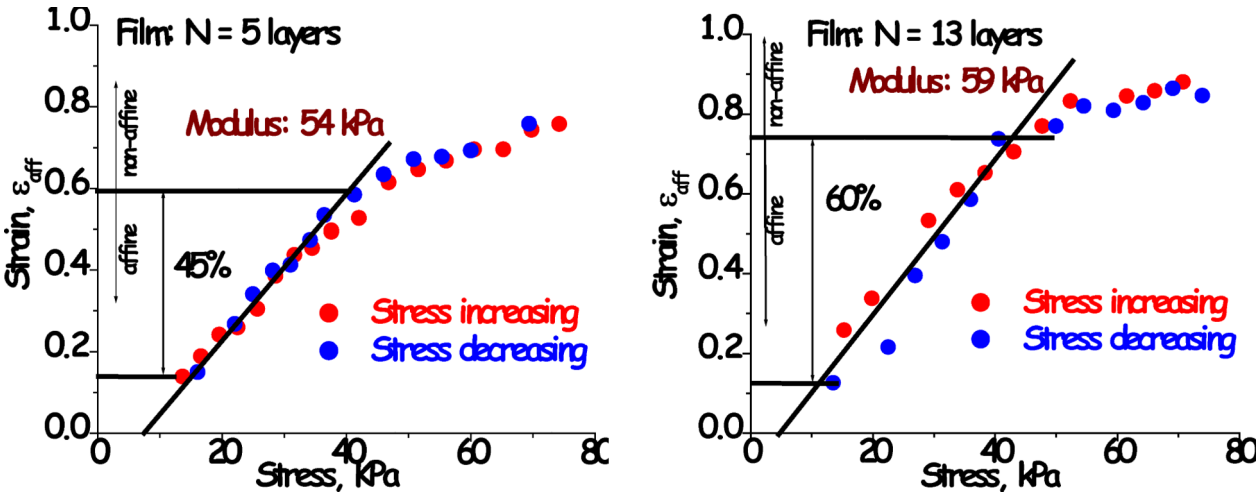

Figure 3:

Typical mechanical behavior of two films calculated from ionic resistance exhibiting the reversible deformation to high compressive strains. Typical behavior of other values of N studied is in SOM, Fig. S1.

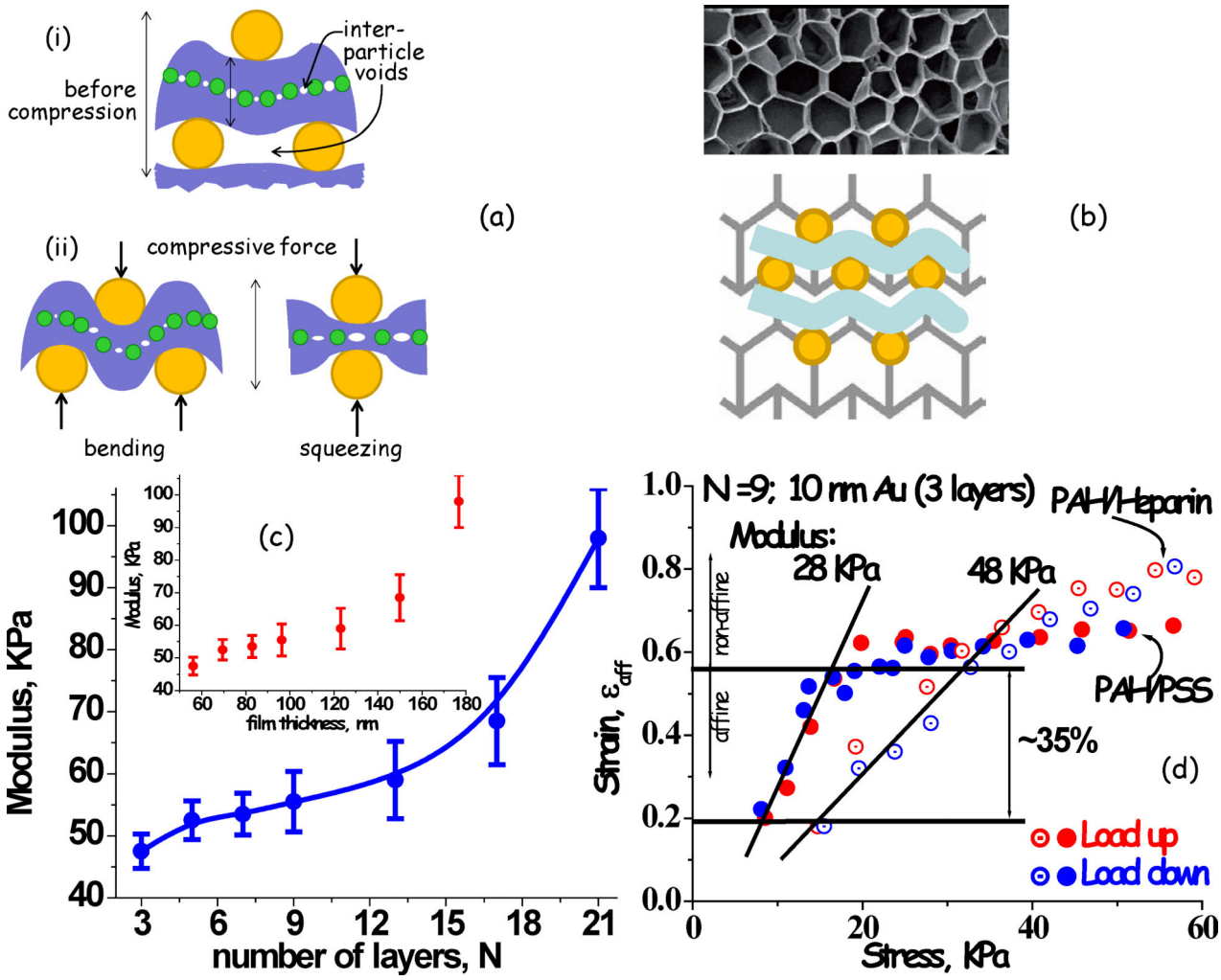

Figure 4:

(a) The two local deformation modes on compression are bending and squeezing of the dielectric layer. The relative dimensions of the schematic are nominally to scale depicting a strain of about 40% in N =7 film. (b) The electron microscope image of the cellular structure of cork. Reproduced with permission from Reference 9. Copyright 2005 Maney Publishing. Idealized model with an overlay of the nanoparticle/polymer layered structure. The width of the image is 350 μm. Reproduced with permission from Reference 10. Copyright 2010 John Wiley and Sons. (c) Effect of N on the modulus of the film based on initial linear region (Fig. 3) averaged over 60 samples. (d) The effect of stiffness of the polymer layer on the modulus of the film made from three layers of 10 nm Au particle monolayer with no CdS particles.

Browse Publications

Grid View List View

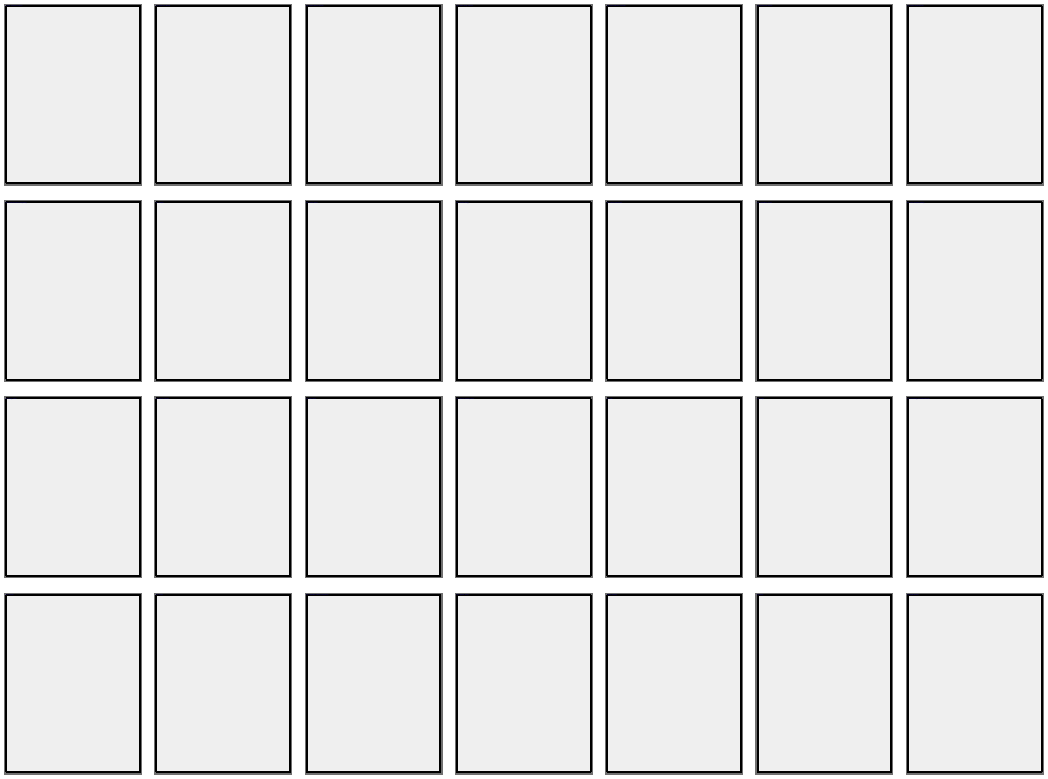

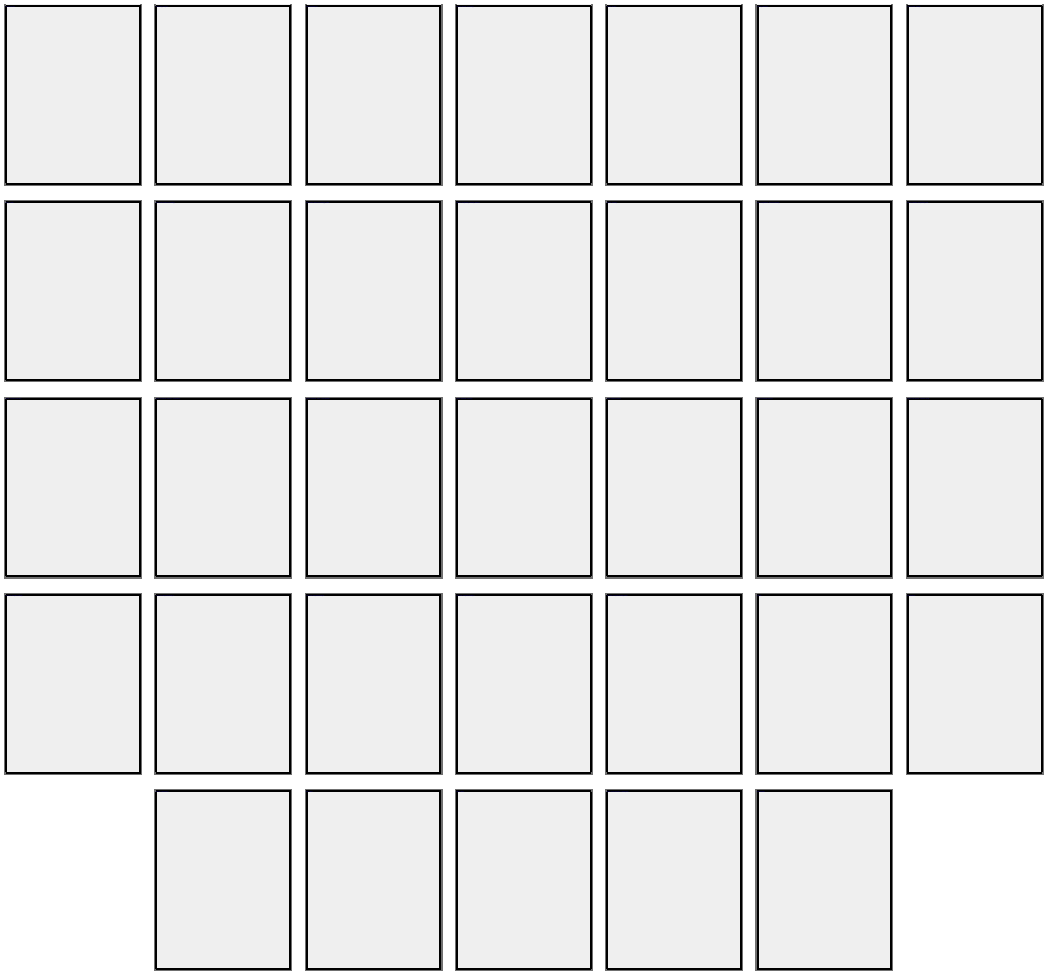

Show More

Teri W. Odom's Personal Story of Discovery

1 year ago

Mireille Kamariza's Personal Story of Discovery

1 year ago

Anne M. Andrews' Personal Story of Discovery

1 year ago

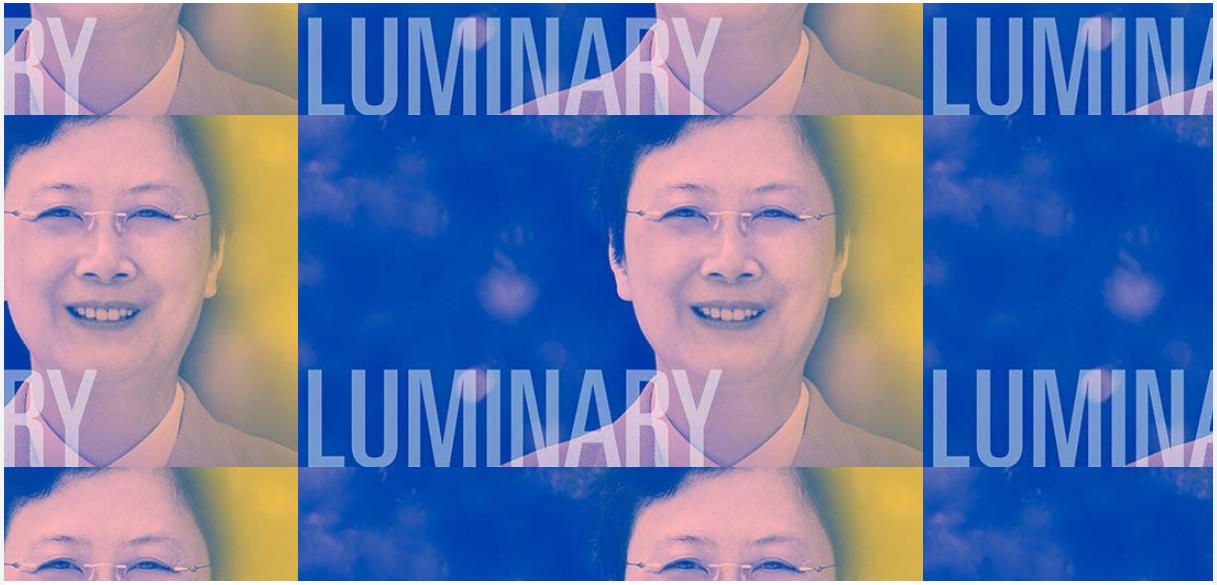

Vivian Yam's Personal Story of Discovery

7 months ago

Trending ACS Articles

1m 3m 6m 12m

ACS Editors' Choice

Based on recommendations from the scientific editors of ACS Journals. See all articles.

About ACS

ACS Publications is dedicated to helping researchers advance scientific excellence to solve global challenges through journals, eBooks, scientific programs, and the newsmagazine Chemical & Engineering News.

Stay Connected...

Connect with us!

Keep current with the latest ASAPs via ACS Mobile app and e-alerts, and follow us for updates on conferences, research highlights, and more.

Facebook

Twitter

WeChat

GET IT ON Google Play

Download on the App Store

Partners

Atypon CHORUS COPE COUNTER Crossref Crossref Similarity Check ORCID Connecting Research and Researchers PORTICO

ACS Publications
Most Trusted. Most Cited. Most Read.

1155 Sixteenth Street N.W.
Washington, DC 20036

Ultra-soft 100 nm Thick Zero Poisson's Ratio Film with 60% Reversible Compressibility

Chieu Nguyen, Vivek Maheshwari[†], Ravi F. Saraf*[,‡]
Department of Chemical and Biomolecular Engineering, ‡ Nebraska Center for Materials and Nanoscience, University of Nebraska-Lincoln, Lincoln, NE 68512; rsaraf2@unl.edu
([†]Present Address: University of Waterloo, Canada)

Supporting Information Online

Two sets of data are presented. All the samples have three layers of Au and two layers of CdS nanoparticles as schematically shown in Fig. 1. The number of polymer layers, N is indicated in the Figure. The Au nanoparticle size is 10 nm (Figure A) and 15 nm (Figure B).

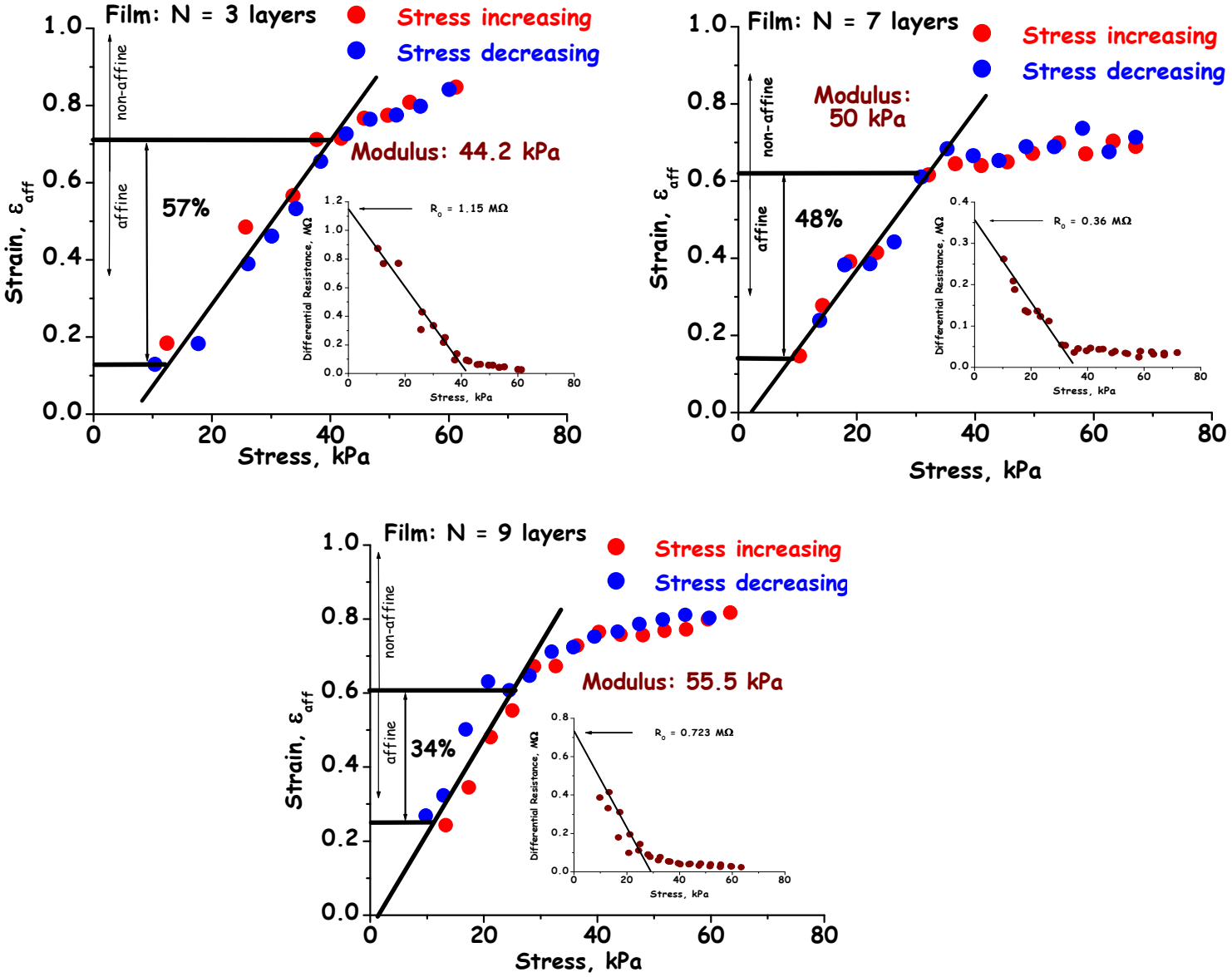

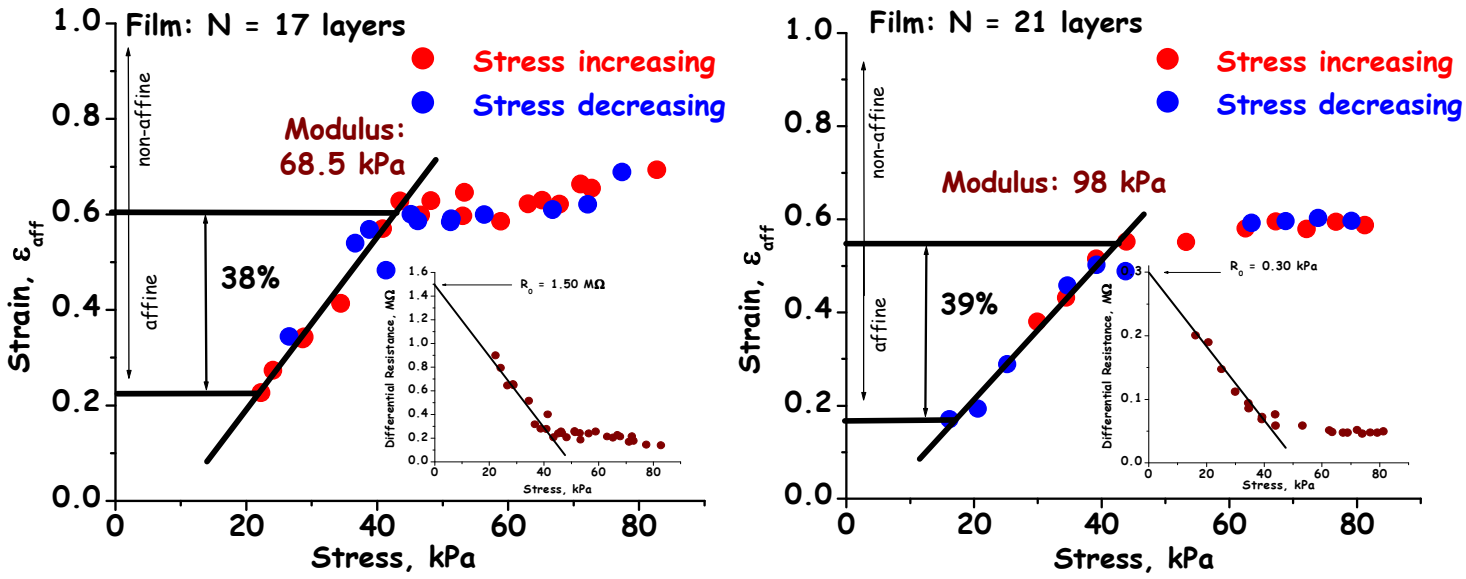

Figure S1: Typical stress-strain curve for N = 3, 7, 9, 17, and 21.

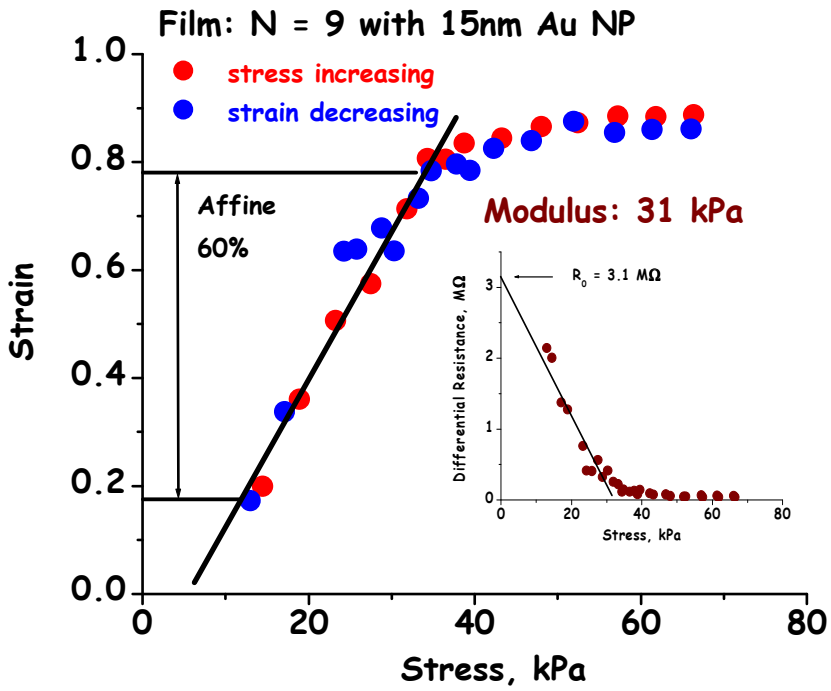

Figure S2: Stress-strain curve for three monolayers of 15 nm Au particle and two monolayers of 3 nm CdS particles.